Fast Display of Illuminated Field Lines

Detlev Stalling, Malte Zöckler, and Hans-Christian Hege

Abstract—A new technique for interactive vector field visualization using large numbers of properly illuminated field lines is presented. Taking into account ambient, diffuse, and specular reflection terms, as well as transparency and depth cueing, we employ a realistic shading model which significantly increases quality and realism of the resulting images. While many graphics workstations offer hardware support for illuminating surface primitives, usually no means for an accurate shading of line primitives are provided. However, we show that proper illumination of lines can be implemented by exploiting the texture mapping capabilities of modern graphics hardware. In this way, high rendering performance with interactive frame rates can be achieved. We apply the technique to render large numbers of integral curves of a vector field. The impression of the resulting images can be further improved by a number of visual enhancements, like color coding or particle animation. We also describe methods for controlling the distribution of field lines in space. These methods enable us to use illuminated field lines for interactive exploration of vector fields.

Index Terms—Vector field visualization, illumination, texture mapping.

1 Introduction

The visual representation of vector fields is the subject of ongoing research in scientific visualization. A number of sophisticated methods have been proposed to tackle this problem, ranging from particle tracing [9], [20], [14] over icon based methods [11], [16] to texture based approaches [4], [3], [5], [19], [12]. A straightforward, powerful, and, therefore, popular technique is to depict field lines, also called integral curves or stream lines. However, using this method, the user is confronted with the following problems. First, on common graphics workstations, field lines either have to be displayed using flat-shaded line segments, impairing the spatial impression of the image, or they have to be represented by polygonal tubes, strongly limiting the number of field lines that can be displayed in a scene. Second, it is usually not quite obvious how to distribute field lines in space in order to get expressive pictures without missing important details of the field. In this paper, we present ideas that can help to overcome both problems.

It is a well-known fact that quality and realism of computer generated images depend, to a high degree, on the accurate modeling of light interacting with the objects in a scene. Shading effects provide perhaps the most important cues for spatial perception. Consequently, much research has been performed to develop realistic illumination and reflection models in computer graphics. A widely used compromise between computational complexity and resulting realism is Phong's reflection model [15], which assumes point light sources, and approximates the most important reflection terms by simple expressions. Traditionally, this model is applied to surface elements. Today, many graphics workstations offer hardware support for this kind of illumination.

• *The authors are with the Konrad-Zuse-Zentrum für Informationstechnik, Berlin, Germany. E-mail: {stalling, zoeckler, hege}@zib.de.*

For information on obtaining reprints of this article, please send e-mail to: transvcg@computer.org, and reference IEEECS Log Number 104721.0.

Phong-type shading models can also be generalized to line primitives in $\mathbb{R}^3$ [2]. Such generalizations have been used to render fur [10] or human hair [1]. However, on current graphics workstations, there is no direct hardware support for the display of illuminated line primitives. Therefore, major parts of the illumination calculations had to be performed in software. In this paper, we present a method to achieve fast and accurate line illumination by exploiting texture mapping capabilities of modern graphics hardware. We apply this new shading technique to visualize large numbers of integral curves in a vector field. By taking into account light reflection, the information content of the resulting images is improved significantly. Thus, the method is of particular importance in scientific visualization. Image quality can be further improved by drawing semitransparent field lines and employing depth cueing. This allows the user to get a better understanding of the spatial structure of a field. Transparency and animation of field lines make it possible to distinguish between forward and backward direction of the field vectors.

The large number of field lines that may be displayed simultaneously also facilitates their placement. We employ statistical methods to select seed points. Given some scalar quantity that loosely describes the degree of interest in the vector field at some location, field lines are placed automatically, such that the relative degree of interest is matched qualitatively. This is possible for user-selected spatial subvolumes, as well as two- and one-dimensional submanifolds.

In scientific visualization, the goal is not to render natural scenes in a photo-realistic way, but to generate images which provide maximal insight into numerical or experimental data. Nevertheless, shading effects are at least as important for the spatial interpretation of artificial images, as in traditional computer graphics. Shading provides the observer with a minimum of realism in a world of cutting planes, isosurfaces, and symbols. Visualization techniques

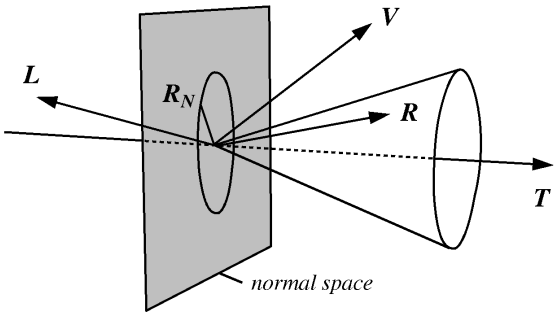

Fig. 1. For line primitives, there are infinitely many possible reflection vectors $\boldsymbol{R}$ lying on a cone around $\boldsymbol{T}$. For the actual lighting calculation, we choose the one contained in the $\boldsymbol{L}$-$\boldsymbol{T}$-plane.

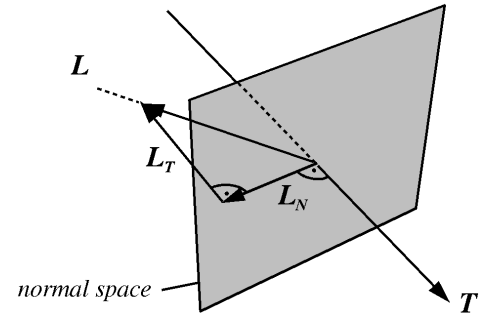

Fig. 2. The light vector $\boldsymbol{L}$ can be decomposed into two orthogonal components, $\boldsymbol{L}_T$ and $\boldsymbol{L}_N$, corresponding to the projection on the line's tangent and normal space, respectively.

can be classified whether they produce 1D, 2D, or 3D geometric primitives, i.e., lines, surfaces, or volumes. Since most graphics workstations provide surface shading calculations only, line-based as well as volume-based visualization methods either were restricted to use flat shading, or illumination calculations had to be performed in software. The hardware texture mapping technique, described in this paper, efficiently breaks this deficiency for the important subclass of line-based renderings.

After discussing illumination of line primitives in more detail, we show, in Section 3, how it can be implemented using texture mapping techniques. In Section 4, we describe several visual enhancements, like use of color, transparency, and depth cueing, as well as animation of field lines. In Section 5, some aspects of numerical field line integration and interpolation are explained. In Section 6, we show how to distribute field lines in space in order to enhance interesting features of a vector field. In Sections 7 and 8, we present results and conclusions.

2 Illumination of Lines in $\mathbb{R}^3$

Surfaces can be characterized locally by a distinct outward normal vector $\boldsymbol{N}$. This normal vector plays an important role when describing the interaction of light with surface elements. In the following, we will shortly review the popular reflection model of Phong. Let $\boldsymbol{L}$ denote the light direction, $\boldsymbol{V}$ the viewing direction, and $\boldsymbol{R}$ the unit reflection vector. $\boldsymbol{R}$ is the vector in the $\boldsymbol{L}$-$\boldsymbol{N}$-plane with the same angle to the surface normal as the incident light. Then light intensity at a particular surface point is given by

$$\begin{aligned} I &= I_{\text{ambient}} + I_{\text{diffuse}} + I_{\text{specular}} \\ &= k_a + k_d\, \boldsymbol{L}\cdot\boldsymbol{N} + k_s(\boldsymbol{V}\cdot\boldsymbol{R})^n. \end{aligned} \tag{1}$$

The first term, a global one, represents the ambient light intensity due to multiple reflections in the environment. The second term describes diffuse reflection due to Lambert's law. Diffuse light intensity does not depend on the viewing vector, i.e., diffuse reflecting objects look equally bright from all directions. The last term in (1) describes specular reflections on a surface. Specular reflections, or highlights, are centered around the reflection vector $\boldsymbol{R}$. The width of the highlights is controlled by the exponent n, also called shininess.

Let us now consider line primitives. In this case, we can no longer define unique normal and reflection vectors. Instead, there are two-dimensional manifolds containing infinitely many possible normal and reflection vectors. Mathematically, lines in $\mathbb{R}^3$ are said to have codimension two. Fortunately, common surface reflection models can be generalized to higher codimensions in a straightforward way. These generalizations have been discussed in detail by Banks [2]. For lines in $\mathbb{R}^3$, the results are quite obvious. From all possible normal vectors, we simply have to select the one which is coplanar to the light vector $\boldsymbol{L}$ and the tangent vector $\boldsymbol{T}$. Taking this particular normal vector, we compute the diffuse reflection term as for surfaces by using (1). Likewise, from all possible reflection vectors, we choose the one coplanar to $\boldsymbol{L}$ and $\boldsymbol{T}$. Again, taking this particular reflection vector, we use (1) to compute the specular reflection term. The relevant vectors for line illumination are illustrated in Fig. 1.

Instead of relying on a specially selected and explicitly calculated normal vector, we would rather like to express diffuse light intensity for line segments solely in terms of $\boldsymbol{L}$ and $\boldsymbol{T}$. Therefore, we first project the light vector into the line's normal and tangent spaces, yielding an orthogonal decomposition $\boldsymbol{L} = \boldsymbol{L}_N + \boldsymbol{L}_T$. As illustrated in Fig. 2, by applying Pythagoras's theorem, we obtain

$$\boldsymbol{L}\cdot\boldsymbol{N} = \left|\boldsymbol{L}_N\right| = \sqrt{1-\left|\boldsymbol{L}_T\right|^2} = \sqrt{1-(\boldsymbol{L}\cdot\boldsymbol{T})^2}. \tag{2}$$

Using similar arguments, we can express the inner product $\boldsymbol{V}\cdot\boldsymbol{R}$ responsible for specular reflection, solely in terms of $\boldsymbol{L}$, $\boldsymbol{V}$, and $\boldsymbol{T}$, i.e., without referring to $\boldsymbol{N}$. First, observe that $\boldsymbol{R}_N = \boldsymbol{L}_N$ and $\boldsymbol{R}_T = -\boldsymbol{L}_T$. We, therefore, have

$$\begin{aligned} \boldsymbol{V}\cdot\boldsymbol{R} &= \boldsymbol{V}\cdot\left(\boldsymbol{L}_N - \boldsymbol{L}_T\right) \\ &= \boldsymbol{V}\cdot\left((\boldsymbol{L}\cdot\boldsymbol{N})\boldsymbol{N} - (\boldsymbol{L}\cdot\boldsymbol{T})\boldsymbol{T}\right) \\ &= (\boldsymbol{L}\cdot\boldsymbol{N})(\boldsymbol{V}\cdot\boldsymbol{N}) - (\boldsymbol{L}\cdot\boldsymbol{T})(\boldsymbol{V}\cdot\boldsymbol{T}) \\ &= \sqrt{1-(\boldsymbol{L}\cdot\boldsymbol{T})^2}\sqrt{1-(\boldsymbol{V}\cdot\boldsymbol{T})^2} - (\boldsymbol{L}\cdot\boldsymbol{T})(\boldsymbol{V}\cdot\boldsymbol{T}). \end{aligned} \tag{3}$$

Here, we have replaced $\boldsymbol{L}\cdot\boldsymbol{N}$ by (2). A similar expression has been used to rewrite $\boldsymbol{V}\cdot\boldsymbol{N}$.

3 Rendering Illuminated Lines

Despite the fact that the illumination equations look the same for lines and surfaces, use of standard hardware shading techniques is impaired, because, for each new light direction, a suitable normal vector has to be computed without utilizing graphics hardware. In the following, we show how (2) and (3) can be effectively evaluated using texture mapping capabilities of modern graphics hardware, thereby avoiding explicit normal vector computation. The technique allows us to achieve high frame rates, even when large numbers of line segments have to be rendered.

3.1 Texture Mapping

We assume we have a graphics API available, similar to OpenGL. In this graphics library, at each vertex, a homogeneous vector of texture coordinates can be specified. Usually, the first components of this vector are taken as indices into a one-, two-, or three-dimensional texture map. A texture map may contain colors and/or transparencies which can be used to modify, in various ways, the original color of a fragment in the graphics pipeline. In addition, it is possible to change texture coordinates using a 4×4 texture transformation matrix. This texture transformation is the key feature which makes it possible to employ texture mapping hardware for shading calculations.

3.2 Diffuse Reflection

Looking at (2), we note that the diffuse light intensity of a line segment is a function of $\boldsymbol{L} \cdot \boldsymbol{T}$ only. Specifying a texture vector $\boldsymbol{t}_0$, equal to the line's tangent vector $\boldsymbol{T}$ at each vertex, this inner product can be computed in hardware using the following texture transformation matrix:

$$M = \frac{1}{2}\begin{pmatrix} L_1 & 0 & 0 & 0 \\ L_2 & 0 & 0 & 0 \\ L_3 & 0 & 0 & 0 \\ 1 & 0 & 0 & 2 \end{pmatrix}$$

The first component of the transformed homogeneous texture vector $\boldsymbol{t} = \boldsymbol{t}_0 M$ then evaluates to

$$t_1 = \frac{1}{2}(\boldsymbol{L} \cdot \boldsymbol{T} + 1).$$

Note that t_1 always lies in the range 0 … 1. Therefore, this value can be used as an index into a one-dimensional texture map $P(t_1)$. The value of the texture map at location t_1 is chosen, such that it resembles the diffuse light intensity corresponding to $\boldsymbol{L} \cdot \boldsymbol{T} = 2t_1 - 1$, namely

$$P(t_1) = I_{\text{diffuse}} = k_d\sqrt{1 - (2t_1 - 1)^2}. \quad (4)$$

By using a texture mode, which takes the color of a fragment to be equal to its texture color $P(t_1)$, we obtain an image which accurately shows line segments diffusely illuminated by a single point light source. While the diffuse color is computed exactly at the vertices of a line segment, minor deviations occur between the vertices. The reason is that texture coordinates are interpolated linearly. This results in unnormalized intermediate tangent vectors. However, the effect is small and not noticeable in practice.

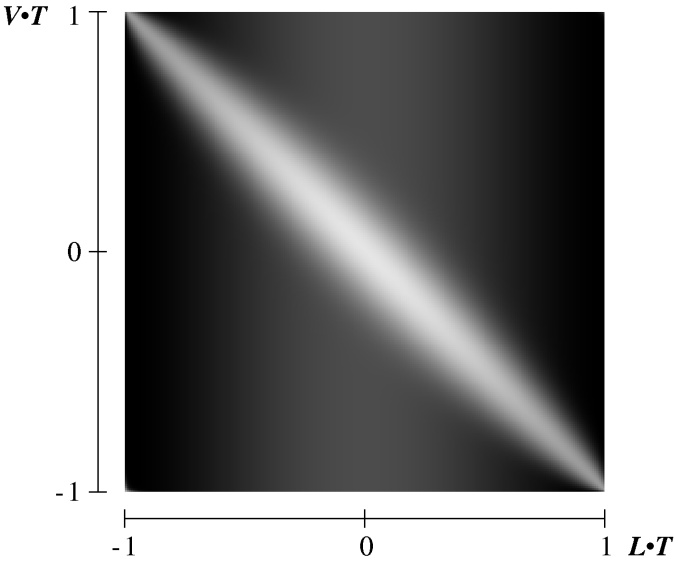

Fig. 3. A two-dimensional texture map used to implement Phong's reflection model for line segments. Parameter values are $k_a = 0.1$, $k_d = 0.3$, $k_s = 0.6$, and $n = 40$.

Notice that only the texture transformation matrix has to be updated when the light direction changes. Vertices and texture coordinates of the line segments remain constant. This makes it possible to make use of OpenGL display lists to further increase rendering speed. Display lists allow one to specify multiple vertex and texture definitions using a single graphics library call.

3.3 Specular Reflection

The specular reflection term not only depends on $\boldsymbol{L} \cdot \boldsymbol{T}$, but also on $\boldsymbol{V} \cdot \boldsymbol{T}$, as can be seen from (3). To compute this additional inner product, we initialize the second column of the texture transformation matrix with the current viewing direction:

$$M = \frac{1}{2}\begin{pmatrix} L_1 & V_1 & 0 & 0 \\ L_2 & V_2 & 0 & 0 \\ L_3 & V_3 & 0 & 0 \\ 1 & 1 & 0 & 2 \end{pmatrix}$$

While the first transformed texture component remains the same, for the second component we now get

$$t_2 = \frac{1}{2}(\boldsymbol{V} \cdot \boldsymbol{T} + 1).$$

In order to obtain the correct light intensity corresponding to $\boldsymbol{L} \cdot \boldsymbol{T} = 2t_1 - 1$ and $\boldsymbol{V} \cdot \boldsymbol{T} = 2t_2 - 1$, we use a two-dimensional texture map $P(t_1, t_2)$. Adding a constant ambient term k_a, as well as the diffuse contribution from (4), we can perform the whole shading calculation for a single light source in texture hardware. Fig. 3 shows an example of a resulting two-dimensional texture map. One can clearly identify the highlight appearing at different angle positions on top of a diffuse background. If no highlight were present, color would not depend on the viewing direction $\boldsymbol{V}$, as stated by Lambert's law.

Again, because interpolated tangent vectors are not normalized, minor errors are introduced between two vertices.

In particular, samples are taken along a linear path in texture space, instead of a slightly curved one. As mentioned above, this effect is not noticeable in practice.

It is worthwhile to note that there is an important special case which allows one to use a one-dimensional texture map, even when specular reflection is present. This is the case of a headlight, i.e., a point light source located at the same position as the camera. In this case, the light vector and viewing vector are identical. Equation (3) simplifies to

$$\boldsymbol{V} \cdot \boldsymbol{R} = 2(\boldsymbol{L} \cdot \boldsymbol{T})^2 - 1.$$

Headlights are quite useful because they always guarantee an adequate illumination of the scene, irrespective of the actual viewing direction. The user does not have to bother with a tedious setup of light conditions. However, as will be shown later, situations also occur where other light positions are favorable.

Of course, it is also possible to use the third column of the texture transformation matrix to compute an additional inner product. This would require the use of a three-dimensional texture map. Three different inner products would allow the illumination of lines by two point light sources located at arbitrary positions, including specular reflection. Alternatively, one might discard specular reflection, and, instead, introduce a third purely diffuse illuminating light source.

3.4 Excess Brightness

Banks [2] pointed out that there is a general problem when illuminating objects with codimension > 1. The overall intensity of an image increases and becomes more uniform, thus disturbing spatial perception. In case of lines in $\mathbb{R}^3$, this can be understood by the following consideration: We know that the normal vector is not a constant one, but is given by the projection of the light vector into the line's normal space. Choosing such a vector means minimizing the angle between the light vector and normal. Therefore, in general, the angle between these two vectors is smaller, compared to the case of a fixed normal. This results in a more uniform brightness than we are used to perceiving in the real world. As suggested by Banks, we compensate the effect qualitatively, by exponentiating the diffuse intensity term:

$$\hat{I}_{\text{diffuse}} = k_d(\boldsymbol{L} \cdot \boldsymbol{N})^p \tag{5}$$

In [2], a value of $p = 4.8$ was proposed. For the images in this paper, we have used a value of $p = 2$, which produced nicer results.

4 Visual Enhancements

There are a number of ways to enhance and modify the rendering of illuminated field lines, as discussed in Section 3. With color coding, it is possible to depict an additional scalar quantity. Transparency can either be used to draw antialiased line primitives to highlight particular regions in space, or to encode the directional sign of a field line. Animation is an even better way to indicate the orientation of a field line. Finally, depth cueing can be used to further improve the understanding of complex spatial structures. In the following section, we will discuss all these topics in more detail.

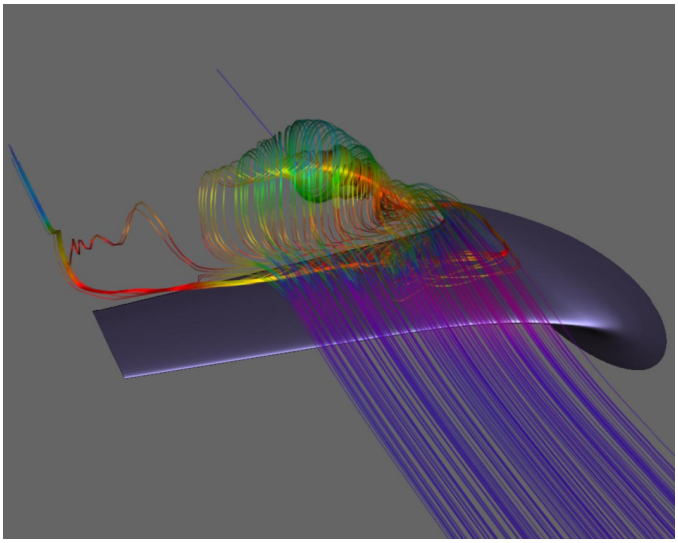

Fig. 4. The image shows the flow around a wing. Color is used to encode velocity magnitude. In contrast to colored flat-shaded lines, illuminated lines clearly reveal the shapes of the vortex structures.

4.1 Color

Color coding is a common method in visualization. Applying color to individual field lines would enable us to depict some scalar quantity, in addition to vector field structure. Such a quantity could be field magnitude, potential strength, or some more unrelated scalar variable, like pressure in a fluid flow. Ideally, we would like to modify the curve's ambient and diffuse color components according to a given color lookup table. However, in our case, colors are taken directly from a texture map. Since we use the same texture map for all field lines, it is not possible to set these components locally in a straight-forward way. Adding a third color dimension to a 2D map doesn't work, because three texture coordinates are needed to define the tangent vector, and an independent fourth one cannot be specified anymore.

Nevertheless, an alternative texture mapping mode can be used to modulate, i.e., multiply, texture color with an object's base color. The latter can be defined for each vertex separately. This yields the desired effect, with the restriction that the specular highlight also gets colored, instead of remaining constant. Fig. 4 suggests that this is only a minor limitation. Despite being differently colored, the highlights can be identified clearly throughout the whole image. They are still important for understanding the spatial structure of the field. At the same time, color accurately encodes an additional scalar variable. The effect of colored highlights is less prominent if bright base colors are used. More accurate images containing constant highlights may be obtained by some kind of two-pass rendering.

4.2 Transparency

Transparency is a powerful concept which can be utilized in a number of ways. However, it requires geometric

primitives to be rendered in a depth-sorted way. We will first discuss some applications of transparency before we describe how to deal with the depth-sorting problem.

4.2.1 Antialiasing

Lines on a raster display may appear rather jagged if a binary scan-conversion algorithm is used. These alias effects can be suppressed effectively by applying coverage masks to modify the transparency of a pixel. This causes the final pixel color to be a mixture of the line's color and the color of the underlying object. This antialiasing method is directly supported by common desktop graphics workstations. It improves image quality significantly, as illustrated in the following figure:

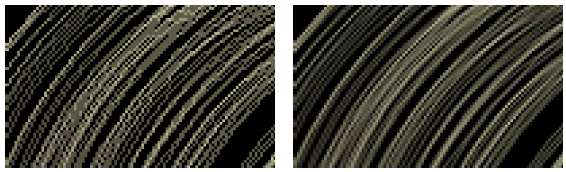

While there are severe aliasing effects in the left image, the right image looks much smoother. Alias effects tend to appear at different locations in successive frames, with slightly different view directions. Since this is very disturbing, antialiasing is even more important for interactive applications and animations. The use of semitransparent line segments allows us to abstain from more expensive antialiasing methods based on supersampling, as provided by high-end graphics workstations.

4.2.2 Highlighting

Transparency can be used to highlight important features of a vector field. In our application, we can use an independent scalar field not only to define color, but also to modify the transparency of a field line at each vertex. In Fig. 5, a simple model of the magnetic field around the earth is shown. While the field of the earth itself is assumed to be a magnetic dipole, the field of the sun is approximated by a constant term. Choosing transparency proportional to the logarithm of vector field magnitude reveals the characteristic dipole structure, and still lets you discern the constant field in the outer region.

4.2.3 Directional Sign

To encode, unambiguously, the directional sign of a vector field, imagine small particles traversing the vector field and leaving a veil of haze. For a stationary field, the particles will just follow the field lines. Assuming that the haze disappears according to an exponential law, opacity, or alpha values, for equidistant points s_n of a field line, are given by

$$\alpha(s_n) = \alpha_0 q^{n-1}. \tag{6}$$

Here, the factor q controls how much of the haze disappears per unit step. A resulting semitransparent field line is illustrated in the following figure:

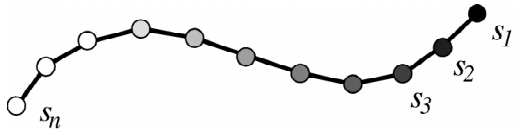

The sign of vector field direction would not become visible if field lines were rendered symmetrically in forward and backward direction. Fig. 10 illustrates the use of transparency to encode the directional sign of a field line. The figure also compares flat shaded and illuminated field lines.

4.2.4 Depth Sorting

Drawing a transparent pixel of opacity α and color C causes the current color in the frame buffer to be updated according to

$$C_{\text{new}} = (1-\alpha)C_{\text{old}} + \alpha C. \tag{7}$$

If multiple transparent objects are present in a scene, the final pixel color depends on the ordering of the individual objects. Correct results are obtained by using a back to front traversal. The situation is simplified if all objects are of equal color, C. In this case, all traversal orders yield the same result. This has been exploited by Max, Crawfis, and Grant [13], who applied flat shaded line bundles for vector field visualization. However, for illuminated lines, color isn't constant. Therefore, individual lines have to be rendered in a depth-sorted way.

In general, it is impossible to achieve an exact depth ordering for extended curves in 3D, because mutual coverings may occur. To minimize such coverings, the seg-

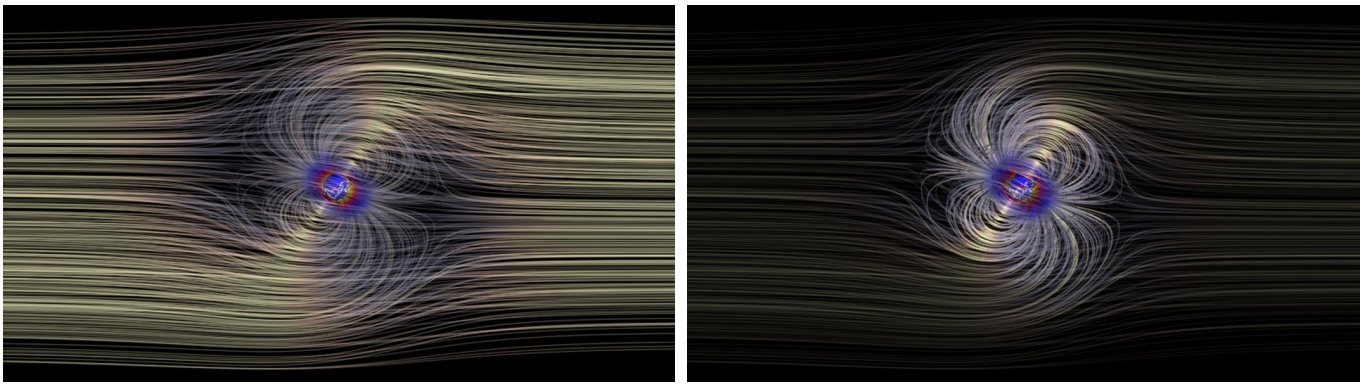

(a) (b)

Fig. 5. (a) Simple model of the magnetic field around the earth. The contribution of the sun is constant, while the earth's field has dipole structure. In (b), transparency is used to emphasize this dipole structure, suppressing the constant contribution in the outer area.

ments of all field lines are sorted and rendered individually. Resorting the line segments for each new view direction can be avoided by using the following simplified algorithm: Three lists of pointers to field line segments are created. The lists are sorted in order of increasing x-, y-, and z-coordinates, respectively. During rendering, the list that most closely resembles the viewing direction is traversed, either from back to front or from front to back. Although this method is not exact, it produces excellent results which cannot be distinguished visually from the exact images. Experiments have shown, that typically only about one percent of all pixels receive somewhat incorrect color values.

4.3 Field Line Animation

Animated particles provide very intuitive means for visualizing vector fields. Following the idea of particles leaving a veil of haze, animation sequences can be computed very easily: Stream lines are created at different times t_i, with an initial length of zero, and initial opacity α_0, as defined by (6). In each time step, all field lines are extended by one point, while opacity of all the points already drawn is modified by the factor q. This gives the illusion of moving particles producing a slowly disappearing veil of haze, like comets. The method is most easily applied to lines consisting of equidistant vertices. In this case, a constant speed motion is obtained, which is well suited to depict the directional sign of the vector field. For variable speed, the length of the field line segments can be chosen proportional to local vector magnitude.

A periodic animation sequence can be created by assuring that the total animation period T is long enough, so that points on a field line can disappear completely within this interval (i.e. $q^T \approx 0$). Then, a field line that has been created at time t_i can be restarted at the same location at time $t_i + T$, since it is no longer visible then. This results in a continuous animation loop of period T.

4.4 Depth Cueing

Depth cueing is a well-established technique to improve the spatial perception of complex three-dimensional scenes. It means that the color of objects is adjusted according to their distance from the camera. The underlying idea is that bright objects of high contrast usually appear closer than dark or washed-out ones. In our context, the method turns out to be especially useful in situations where illuminated field lines are arranged such that they constitute surface-like structures. Since the illumination model does not distinguish between inside and outside, sometimes the spatial structure of such pseudosurfaces may not be clear on the first sight. Depth cueing helps to identify near and far parts of the geometry, and, therefore, improves spatial perception. This becomes obvious by comparing Fig. 6b and Fig. 6c.

The improvement is even more important when objects are rotated interactively. Although parts of the scene may be fully occluded when depth cueing is strong, they become visible when viewed from another direction.

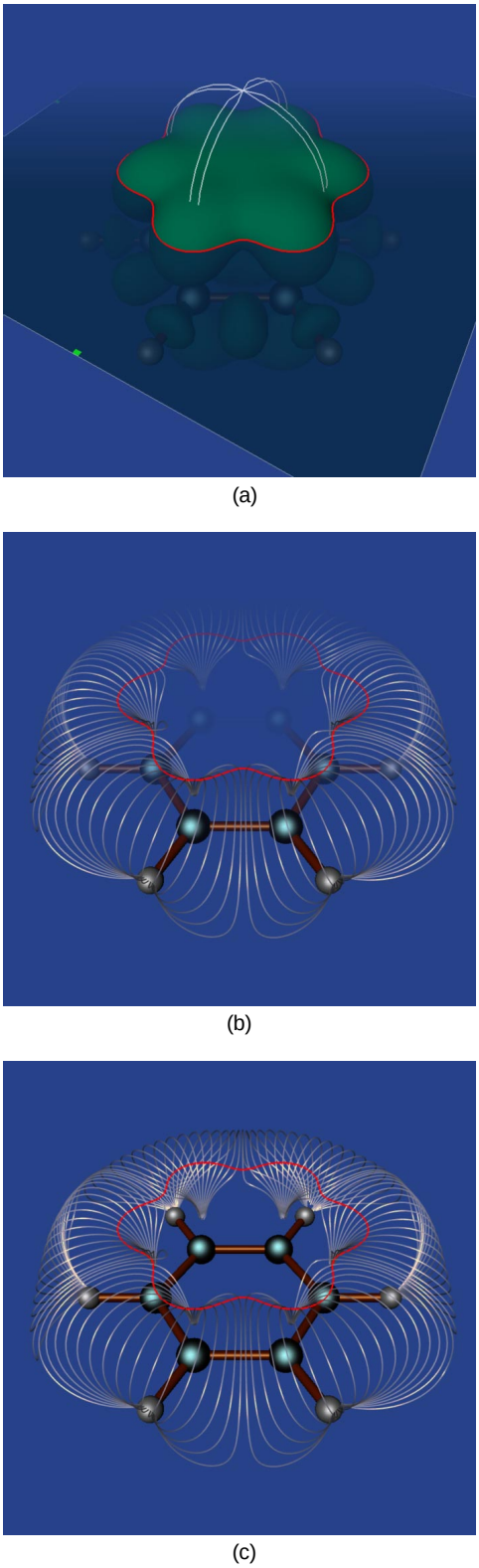

(a) (b) (c)

Fig. 6. A cutting plane is used to interactively define a cut through an isopotential surface (a). Seed points are placed on the resulting intersection line. In (a) and (b), depth cueing has been applied. This helps to improve spatial impression, especially in interactive applications.

5 Field Line Integration

For numerical field line integration, we use a fourth-order Runge-Kutta method with error monitoring and adaptive step size control, as described in [19]. Use of an adaptive method allows us to control the error of the solution. Such methods are also necessary to detect singularities. At these points, field line integration has to be terminated.

Singularities, i.e., sinks and sources, commonly occur, for example, in electrostatic fields. Examples are shown in Figs. 6 and 8.

A common problem with adaptive integrators is that the step sizes usually are so large that the resulting curve cannot be approximated by straight line segments anymore. Instead, additional samples have to be computed between the solution vectors. These are obtained by evaluating an interpolation polynomial whose degree should conform to the order of the integrator. For a fourth-order integrator, cubic Hermite interpolation is an appropriate choice [8]. It retains the exact values of the tangent vectors at the endpoints of an interval, in addition to the location of the endpoints itself. The tangent vectors, themselves, are interpolated by a quadratic polynomial. To quickly evaluate the interpolation polynomials at equidistant steps, we are using forward differences.

The step size of an adaptive integrator is closely related to the curvature, of the solution curve. In areas of high curvature, small steps are taken, while in areas of little curvature large steps are taken. Therefore, it makes sense to subdivide each interval using an equal number of intermediate samples. The number of intermediate samples determines how closely the original geometry is approximated. We obtained good results with three to five intermediate samples.

Instead of precomputing intermediate samples during field line integration, it is also possible to defer evaluation of the interpolation polynomials until rendering. OpenGL provides means for sampling a polynomial curve at equidistant locations. Instead of specifying vertices or texture coordinates directly, so-called evaluators can be used to compute these quantities from a polynomial. For this, the curve has to be specified in terms of linearly independent Bernstein polynomials. For a cubic curve, the Bernstein polynomials are $(1-u)^3$, $3(1-u)^2u$, $3(1-u)u^2$, and u^3. The advantage of letting OpenGL interpolate the intermediate samples is that the number of subdivisions can be easily changed without any recomputation. For example, it would be possible to adjust the resolution to the current view (level of detail). However, in general, faster rendering times are obtained by computing the intermediate samples in a preprocessing step, and then drawing the field lines directly as straight line segments. Only for a large number of subdivisions (> 25) OpenGL's evaluator interface becomes preferable.

In some situations, it is also desirable to render the field lines with equidistant samples. For example, if an independent scalar field is used to obtain color or opacity values for each vertex, the required resolution doesn't depend on field line curvature alone, but also on the characteristics of the scalar field. If nothing is known about this field, using equidistant samples seems to be the best choice.

6 Seed Point Selection

The proper choice of seed points for field line integration is a common problem in vector field visualization. On the other hand, the fast texture based rendering technique, described above, allows us to generate images with thousands of lines at interactive rates. This means that the positioning of an individual field line becomes less important. This allows us to apply statistical methods for distributing seed points in the data volume.

It should be mentioned that, ideally, the distribution of the field lines itself should be controlled, rather than the distribution of seed points. If the directional field has a nonvanishing divergence, field line density will not remain constant. Instead, field lines will run together in some areas, resulting in an increased local density, or they will expand in other areas, resulting in a decreased local density. These variations are less dominant if the total length of a line is limited, and if the field lines are integrated an equal distance in forward and backward direction. Using this approach, we obtained reasonable results with just controlling seed point density, instead of field line density. More elaborate strategies compute an optimized distribution by taking into account some kind of repulsion between different lines, as described for the 2D case in [18]. However, this is a rather expensive computational process.

6.1 The Interest Function

Often, it is intuitive to have a field line distribution proportional to some scalar quantity p. Such a field p may be interpreted as the degree of interest the user wants to put in a region. For example, a constant p would result in a homogenous distribution of seed points, while a value of p proportional to vector magnitude would emphasize regions of large field strength.

In general, it is not a trivial task to find a good interest function p. For example, in electrostatic data sets, field strength often varies over several orders of magnitude. Instead of choosing p exactly proportional to field strength, we would rather like to have a more homogenous distribution which resembles vector field magnitude only qualitatively. Such an effect can be obtained using a histogram equalization approach. This technique is well known from the image processing literature [7], but, in our case, may also be used to modify the degree of interest p in a suitable way. By subdividing the whole data volume into uniform cells, we define a sum histogram in the following way:

$$S(p) = \frac{\text{number of cells with } p_i < p}{\text{total number of cells}} \tag{8}$$

Based on the sum histogram, we can assign each cell a new equalized degree of interest p_i' by

$$p_i' = S(p_i). \tag{9}$$

Of course, other probability distributions could be useful to emphasize special features of the field. We have implemented a symbolic interface which allows us to specify p_i as a function of any given set of scalar fields. Within this interface, functions, like logarithm or square root, as well as threshold operators, can be used to specify the degree of interest p.

6.2 Seed Volumes

To actually generate seed points with a given density p, we again subdivide the data volume into n uniform cells. For each cell, we compute a value p_i, describing the local degree of interest for that cell. The accumulated degree of interest is defined by

$$\omega_i = \sum_{j=1}^{i} p_j \,. \tag{10}$$

We assume all cells being arranged in a sequence are based on some arbitrary numbering. We randomly choose cells with a probability proportional to p_i. This is done by taking a random number r uniformly distributed in the range 0 … ω_n. The first value, $\omega_i > r$, determines which cell is taken.

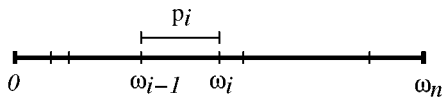

Within a selected cell, we place a new seed point at a random position. Because the values ω_i are monotonously increasing, the cell lookup procedure has a complexity of $O(\log(n))$, and, therefore, can be performed quite fast.

To get an overview of the global field structure, it is a good idea to choose an initial seed volume that fully encloses the data set. The user then may further constrain the seed volume. For this, we use so-called draggers, provided by the Open Inventor graphics toolkit. Draggers are interactive components that may be translated and rescaled directly in a three-dimensional scene. They provide a very flexible and intuitive interface. An example of an Inventor-style selection box is shown in Fig. 9.

6.3 Seed Surfaces

Instead of using seed volumes, field lines may also be started on two-dimensional manifolds. For example, to visualize the structure of an electrostatic field, seed points may be distributed on an isopotential surface. This method is of particular interest, since an electrostatic field is always oriented perpendicular to such a surface. It may reveal important features of the field.

We assume a surface S to be given by a set of triangles. To distribute n_p seed points homogenously on S, we first determine how many points have to be placed in a particular triangle T_i of the surface. The larger a triangle is, the more seed points it should contain, i.e.,

$$n_i = \frac{Area(T_i)}{Area(S)} n_p. \tag{11}$$

We always generate at least $\lfloor n_i \rfloor$ points in each triangle T_i. To deal with noninteger numbers n_i, an additional point is generated with a probability given by the fractional part $n_i - \lfloor n_i \rfloor$. Again, seed point density may also be chosen proportional to some interest function $p(x)$ defined on the manifold. In this case, (11) has to be replaced by

$$n_i = \frac{\int_{T_i} p(x)dA}{\int_S p(x)dA} n_p. \tag{12}$$

Inside a triangle, all points are distributed uniformly. This is a reasonable approximation also for nonconstant density functions $p(x)$, if the triangles are small enough. To obtain a uniform point distribution within a triangle, we choose two uniform numbers u and v in the range [0..1]. If $u + v > 1$, then $u := 1 - u$ and $v := 1 - v$ are used instead. The final position of a point inside a triangle is given by $\boldsymbol{P} = \boldsymbol{A} + u(\boldsymbol{B} - \boldsymbol{A}) + v(\boldsymbol{C} - \boldsymbol{A})$, where $\boldsymbol{A}$, $\boldsymbol{B}$, and $\boldsymbol{C}$ are the vertices of the triangle. If the final distribution is not sufficiently homogeneous, the points can be moved on the surface using a point-repulsion approach, as described in [17]. An example of field lines placed uniformly on isopotential surfaces is shown in Fig. 7. The image reveals the structure of the electrostatic field of a water molecule.

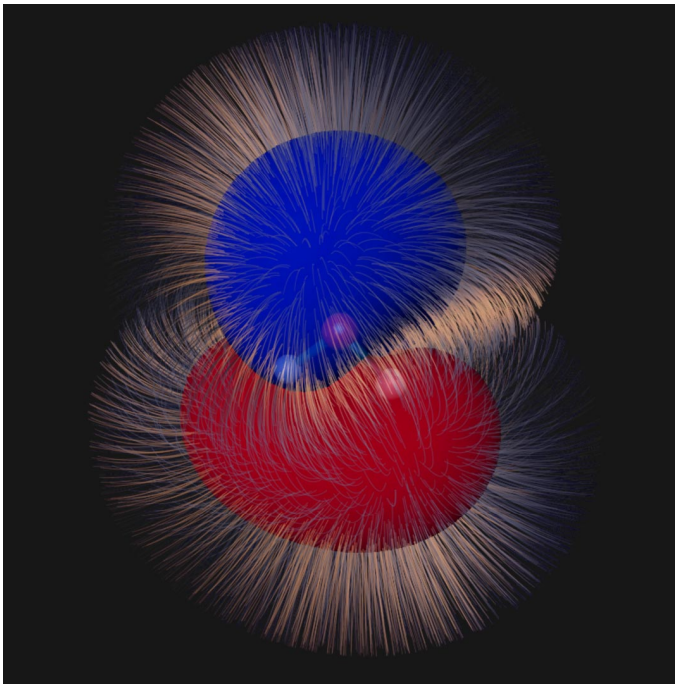

Fig. 7. Electrostatic field of a water molecule. Seed points are distributed uniformly on two isopotential surfaces. In this image, a directional light shining from the upper right is used for illumination. If light and view direction were coincident, it would be hard to identify lines facing the camera.

Instead of placing seed points on complex geometries, like isosurfaces, we have also implemented a small surface probe, which can be moved and rotated interactively within the scene. Again, we utilized Open Inventor components. An example of a surface probe, together with a box-style dragger, is shown in Fig. 9.

6.4 Seed Lines

Another way of seed point selection is to start field lines on one-dimensional manifolds, i.e., lines. Instead of using simple geometric primitives, like straight line segments or circles, such manifolds may be defined conveniently by intersecting surfaces with a cutting plane. Again, isosurfaces are suitable candidates for such an operation. We use draggers defined in Open Inventor to implement a cutting plane which can be translated and rotated easily in a three-dimensional scene. Open Inventor also provides a so-called triangle callback action, which allows us to actually compute the intersection.

An example of a set of field lines distributed on a one-dimensional manifold is depicted in Fig. 6. The curve has been defined by intersecting an isosurface with a cutting plane. This way of placing seed points is especially suited to

emphasize possible symmetries in a field. The image also shows the effect of depth cueing, as discussed in Section 4.4.

7 Implementation and Results

The algorithms presented in this paper have been implemented in C++ by subclassing the Open Inventor toolkit. Using Inventor makes it easy to display illuminated field lines in combination with other geometries. The rendering code itself is built on top of the OpenGL graphics library. It is embedded into an object-oriented visualization system developed at Konrad-Zuse-Zentrum für Informationstechnik, in Berlin. The object-oriented design allows us to process 3D vector fields, defined in various ways, by using a common interface. Examples are analytically defined fields (Fig. 5), fields defined on curvilinear grids (Fig. 4), or fields on regular grids, as in the molecular datasets.

We have applied our methods to visualize vector fields from various disciplines, such as computational fluid dynamics, quantum chemistry, and astrophysics. In most cases, the default values for seed point distribution provide a good first impression of the vector field. The fast rendering speed offers the possibility to interactively rotate and zoom the geometry. This is an important feature for understanding the complex vector field structures. The precomputation time needed for field line integration and depth-sorting was less than four seconds in all of our examples. All performance measurements have been done on an SGI Indigo^2 with Maximum Impact Graphics and 250 MHz R4400 CPU.

Fig. 4 shows the air flow around a wing, obtained from a CFD simulation. The vector field is defined on a curvilinear grid. Color is used to encode velocity magnitude. Blue depicts regions of high velocity, while yellow and red show slowly flowing parts of the field. The scene contains 14,200 line primitives, and can be rendered at a frame rate of 25 frames per second. The rendering time for the polygonal wing model is negligible, compared to the time needed for line drawing.

In Fig. 5, a simple model of the magnetic field around the earth is shown. This field is given analytically. Transparency modulation is used to enhance the dipole structure of the earth field, as described in Section 4.2 (27,000 lines, 15 fps).

Fig. 8 shows the electrostatic field of a benzene molecule. The field is computed using the NAO-PC method (Natural Atomic Orbitals—Point Charge). This quantum-classical method approximates atomic orbitals by a set of discrete fractional point charges. The location of some of these point charges can be clearly identified in the images (19,100 lines, 18 fps).

An example of a velocity field from a CFD application is shown in Fig. 9. The data represents a fluid flow over a backward facing step. The turbulent region behind the step is characterized by a very complex field structure. A 3D dragger is used to highlight this part of the field. In addition some field lines are seeded on a probe-surface (25,000 lines, 15 fps).

Rendering speed can be further increased, either by reducing the per vertex call overhead, or by improving cache coherency. We observed performance gains of 10-20 percent by making use of OpenGL display lists. In a display list, multiple graphics commands are arranged in a way optimized to feed the graphics pipeline. By using display lists, cache misses should be minimized. However, due to the depth-sorting approach, in our case, six independent display lists have to be generated. Therefore, the start-up time needed to generate the lists as well as the memory overhead, usually outweighs the performance gain. Alternatively, the vertex array, or packed vertex array extensions of SGI's OpenGL implementation, might be used to improve performance. These extensions are specifically designed to reduce the per vertex call overhead. They involve memory and start-up overheads similar to display lists.

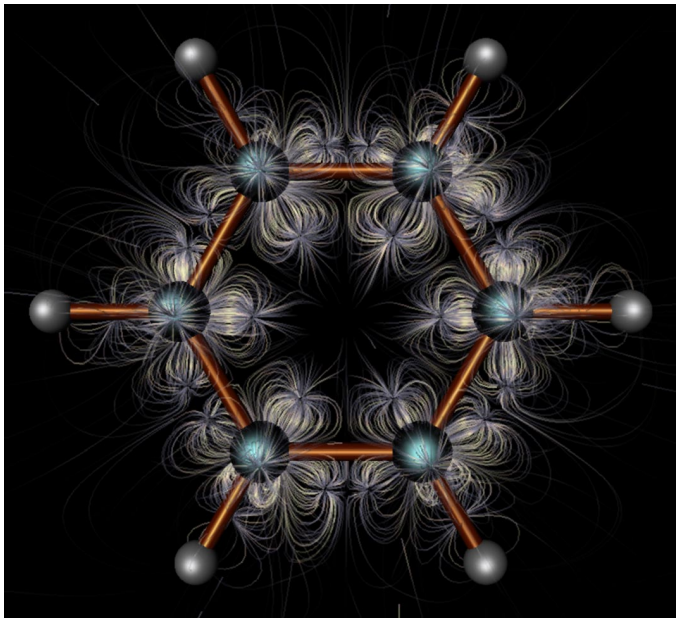

Fig. 8. Electrostatic field of a benzene molecule. The field line seeds were distributed proportionally to field strength.

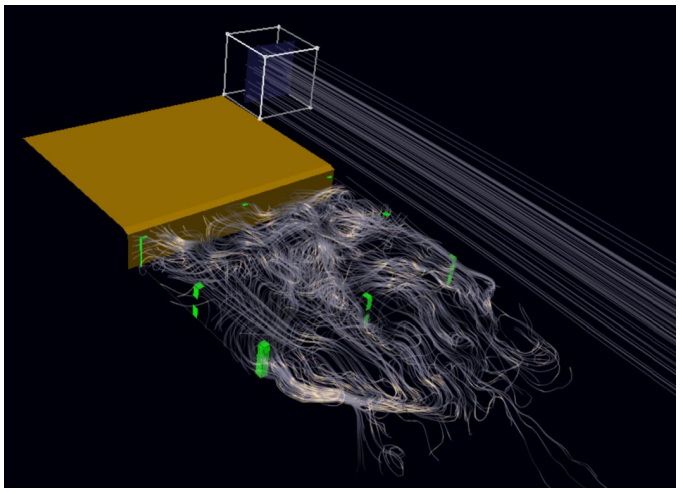

Fig. 9. Velocity field from a CFD simulation. Open Inventor draggers are used to define a seed volume (turbulent region) and a surface probe (upper part).

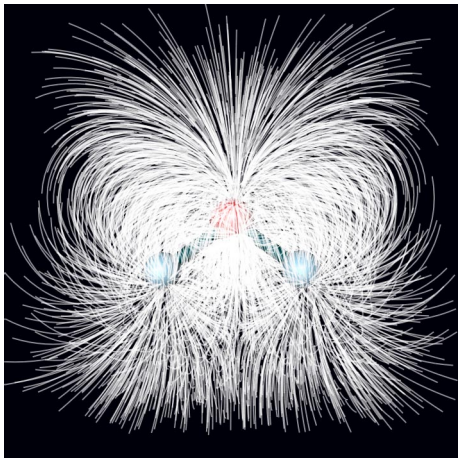

(a)

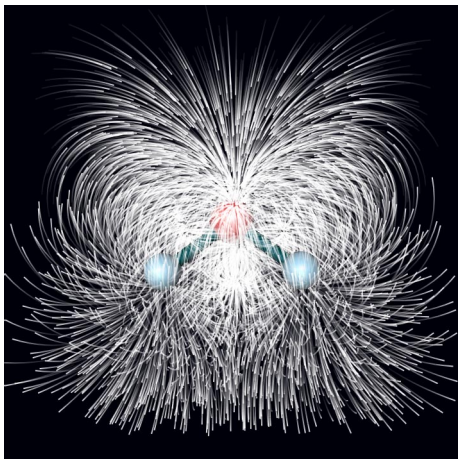

(b)

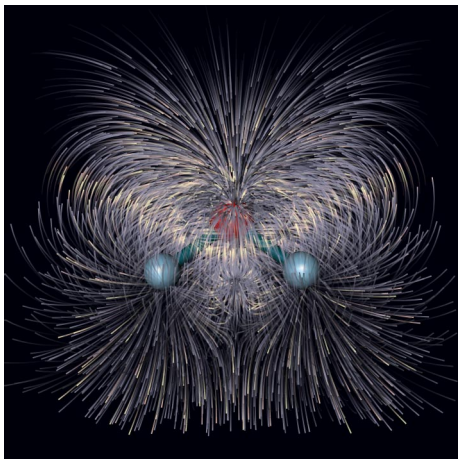

(c)

Fig. 10. In (a), fully opaque, flat shaded field lines are drawn. In (b) and (c), transparency is used to encode the directional sign of the field lines. Finally, (c) shows the effect of proper illumination.

8 Conclusion

The visual representation of 3D vector fields is one of the current challenges in scientific visualization. Of particular interest are methods that provide an overview of the global field structure and also depict fine details.

In this paper, we have presented a fast method for visualizing 3D vector fields based on the display of field lines, i.e., integral curves of the field. The method gives a good impression of the field structure, and enables us to visually resolve rather fine details, like small vortices. A texture mapping technique is used to accurately illuminate the field lines. Light reflection on field lines improves spatial perception, and, thereby, facilitates the understanding of the inner structure of a field.

We have shown how high quality field line images can be generated at interactive speed by using hardware supported texture mapping. This offers new opportunities for interactive visualization. By using a simple Monte-Carlo method, lines are placed automatically such that the relative degree of interest, defined by some scalar field, is matched qualitatively.

An interesting topic of further research is the improvement of seed point selection strategies so that characteristic features of the field can be detected and enhanced automatically. Moreover, the application of line illumination to time dependent vector fields is an important task. In this case, particle paths, or streak lines, should be used in favor of field lines.

References

[1] K. Anjyo, Y. Usami, and T. Kurihara, "A Simple Method for Extracting the Natural Beauty of Hair," *Computer Graphics*, vol. 26, pp. 111-120, July 1992. (*Proc. ACM Siggraph '92*).

[2] D.C. Banks, "Illumination in Diverse Codimensions," *Computer Graphics Ann. Conf. Series*, pp. 327-334, July 1994. (*Proc. ACM Siggraph '94*, Orlando, Fla.)

[3] B. Cabral and L. Leedom, "Imaging Vector Fields Using Line Integral Convolution," *Computer Graphics*, vol. 27, pp. 263-272, Aug. 1993. (*Proc. ACM Siggraph '93*, Anaheim, Calif.)

[4] R. Crawfis and N. Max, "Textured Splats for 3D Scalar and Vector Field Visualization," *Proc. Visualization '93*, G. Nielson and D. Bergeron, eds., pp. 261-272. IEEE CS Press, 1993.

[5] L.K. Forsell, "Visualizing Flow over Curvilinear Grid Surfaces Using Line Integral Convolution," *Proc. Visualization '94*, D. Bergeron and A. Kaufman, eds., pp. 240-247. IEEE CS Press, 1994.

[6] A. Van Gelder and J. Wilhelms, "Interactive Animated Visualization of Flow Fields," *Proc. ACM Workshop Volume Visualization*, pp. 47-54, 1992.

[7] R.C. Gonzales and P. Wintz, *Digital Image Processing*, second edition, pp. 146-152. Addison Wesley, 1987.

[8] E. Hairer, S.P. Nørsett, and G. Wanner, *Solving Ordinary Differential Equations I, Nonstiff Problems*. Berlin: Springer Verlag, 1987.

[9] A.J.S. Hin and F.H. Post, "Visualization of Turbulent Flow with Particles," *Proc. Visualization '93*, pp. 46-52. IEEE CS Press, 1993.

[10] J. Kajiya and T. Kay, "Rendering Fur with Three Dimensional Textures," *Computer Graphics*, vol. 26, pp. 271-280, July 1989. (*Proc. ACM Siggraph '89*)

[11] W.C. de Leeuw and J.J. van Wijk, "A Probe for Local Flow Field Visualization," *Proc. Visualization '93*, G. Nielson and D. Bergeron, eds., pp. 39-45. IEEE CS Press, 1993.

[12] W.C. de Leeuw and J.J. van Wijk, "Enhanced Spot Noise for Vector Field Visualization," *Proc. Visualization '95*, G. Nielson and D. Silver, eds., pp. 233-239. IEEE CS Press, 1995.

[13] N. Max, R. Crawfis, and C. Grant, "Visualizing 3D Velocity Fields Near Contour Surfaces," *Proc. Visualization '94*, D. Bergeron and A. Kaufman, eds., pp. 248-255. IEEE CS Press, 1994.

[14] K.-L. Ma and P.J. Smith, "Virtual Smoke: An Interactive 3D Flow Visualization Technique," *Proc. Visualization '92*, pp. 46-52. IEEE CS Press, 1992.

[15] B.-T. Phong, "Illumination for Computer Generated Pictures," *Comm. ACM*, pp. 311-317, June 1975.

[16] F.J. Post, T. van Walsum, and F.H. Post, "Iconic Techniques for Feature Visualization," *Proc. Visualization '95,* G. Nielson and D. Silver, eds., pp. 288-295. IEEE CS Press, 1995.
[17] G. Turk, "Generating Textures on Arbitrary Surfaces Using Reaction-Diffusion," *Computer Graphics,* vol. 25, no. 4, pp. 289-298. (*Proc. Siggraph '91,* Las Vegas)
[18] G. Turk and D. Banks, "Image-Guided Streamline Placement," *Computer Graphics Ann. Conf. Series,* pp. 453-460, *1996*. (*Proc. ACM Siggraph '96,* New Orleans)
[19] D. Stalling and H.C. Hege, "Fast and Resolution Independent Line Integral Convolution," *Computer Graphics Ann. Conf. Series,* pp. 249-256, 1995. (*Proc. ACM Siggraph '95,* Los Angeles)
[20] J.J. van Wijk, "Rendering Surface-Particles," *Proc. Visualization '92,* pp. 54-61. IEEE CS Press, 1992.

Detlev Stalling studied physics at the University of Osnabrück and the Free University of Berlin, where he received his MS degree in 1993. Afterward, he joined the Konrad-Zuse-Zentrum Berlin (ZIB) as a research scientist in the scientific visualization department. His research interests include accurate visualization methods, geometric modeling, and image processing. Currently, he is working on his PhD thesis on visual methods for analyzing vector fields.

Malte Zöckler studies physics at the Technical University of Berlin, and will finish his diploma in the field of molecular dynamics in the summer of 1997. He has been a member of the Scientific Visualization Research Group at ZIB since 1994. His current research interests include visualization of physical data sets, human/computer interfaces, interaction, 3D animation, and image and volume segmentation.

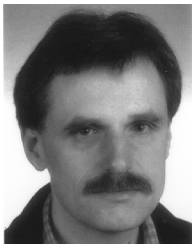

Hans-Christian Hege studied physics at the Free University Berlin. He is head of the scientific visualization department at Konrad-Zuse-Zentrum, Berlin (ZIB). From 1984-1989, he was a research assistant in the Physics Department, working in quantum field theory and numerical physics. He is a cofounder of Mental Images and the Gesellschaft für digitale Simulation (GDS). From 1986 to 1989, he worked as a researcher at Mental Images and managing director at GDS. He has been with ZIB since 1989, first as scientific consultant, and then as director of the visualization and parallel computing department. His current research interests are in computer graphics, scientific visualization, biomedical computing, and physics.